AIP | Physics of Plasmas

Slowly varying envelope kinetic simulations of pulse amplification by Raman backscattering

Min Sup Hur, Gregory Penn, Jonathan S. Wurtele, and Ryan Lindberg

Citation: Physics of Plasmas (1994-present) **11**, 5204 (2004); doi: 10.1063/1.1796351

View online: http://dx.doi.org/10.1063/1.1796351

View Table of Contents: http://scitation.aip.org/content/aip/journal/pop/11/11?ver=pdfcov

Published by the AIP Publishing

Slowly varying envelope kinetic simulations of pulse amplification by Raman backscattering

Min Sup Hur, Gregory Penn, Jonathan S. Wurtele, and Ryan Lindberg
Lawrence Berkeley National Laboratory, University of California, Berkeley, California 94720

(Received 29 April 2004; accepted 28 July 2004; published online 22 October 2004)

A numerical code based on an eikonal formalism has been developed to simulate laser-plasma interactions, specifically Raman backscatter (RBS). In this code, the dominant laser modes are described by their wave envelopes, avoiding the need to resolve the laser frequency; appropriately time-averaged equations describe particle motion. The code is fully kinetic, and thus includes critical physics such as particle trapping and Landau damping which are beyond the scope of the commonly used fluid three-wave equations. The dominant forces on the particles are included: the ponderomotive force resulting from the beat wave of the forward and backscattered laser fields and the self-consistent plasma electric field. The code agrees well, in the appropriate regimes, with the results from three-wave equations and particle-in-cell simulations. The effects of plasma temperature on RBS amplification are studied. It is found that increasing the plasma temperature results in modification to particle trapping and the saturation of RBS, even before the onset of Landau damping of the plasma wave. This results in a reduction in the coupling efficiency compared to predictions based on the three-wave equations. © *2004 American Institute of Physics*.
[DOI: 10.1063/1.1796351]

I. INTRODUCTION

Ultrashort, intense laser pulses are an important tool in the study of high-energy density plasmas,[1,2] laser wake-field accelerators,[3,4] and fast ignition in inertial confinement fusion (ICF) (Refs. 1, 2, and 5). Material breakdown limits the achievable intensity of the conventional chirped-pulse amplification (CPA) scheme.[6] Recently, a novel scheme of amplifying a short laser pulse in a plasma was proposed by Shvets *et al.* in which a long, counterpropagating pump laser transfers its energy to a short seed pulse via the Raman backscattering (RBS) instability.[7] Raman amplification of a pulse up to 10^{17} W/cm^2 prior to focusing may be possible[8] using this scheme. This is a much higher limit than that of CPA,[6] where the maximum pulse intensity is restricted, because of damage to diffraction gratings, to roughly 10^{12} W/cm^2 at $\lambda \sim 1$ μm. Theoretical analysis of Raman amplification using the three-wave equations[8,9] has focused primarily on the π-pulse regime,[8] where a seed pulse is amplified to an intensity much higher than that of the pump while it is compressed in time.

Most of the analytic and simulation work on Raman amplification has concentrated on the cold plasma case; experimental plasmas, on the other hand, always have some nonzero temperature. The naive intuition is that if the plasma temperature is sufficiently low so that Landau damping is ignorable (which is experimentally possible), the cold plasma simulation and analysis will be valid. However, a warm, thermal plasma is more prone to wave breaking than is a cold one.[10] This, in turn, leads to particle trapping in the ponderomotive wave bucket. There exists a rich body of physics in the trapped-particle regime, including saturation of driven Langmuir waves,[11] reduced damping,[12] and nonlinear frequency shifts[13] of undriven waves. Raman amplification in this regime cannot be accurately modeled by the three-wave equations, when temperature and kinetic effects become important. Particle-in-cell (PIC) simulations in the wave breaking regime,[14] for example, show much less efficient pump depletion than fluid simulation. The kinetic effects can be self-consistently included in PIC simulations, but only at a high computational cost, especially when two- or three-dimensional systems are considered. Even in the one-dimensional case, a systematic study is challenging at high temperature, since a large number of particles should be used to reduce the numerical thermal noise.

This paper first describes an efficient numerical simulation of RBS, one that employs envelope equations for the two lasers (seed and pump) and a fully particlelike description for the plasma. The coupling between particles and the laser envelopes is readily found from the conservation of the canonical momentum (so that the transverse current is determined by the laser vector potentials) and averaging over the fast electromagnetic oscillation phase. This leaves eikonal equations for the laser envelopes and one momentum equation for each particle. Due to the averaging, the simulation time step need not resolve the laser frequency; it has only to resolve the plasma wave frequency ω_p. The simulation time is thus faster than a full PIC method by a factor of order ω/ω_p, where ω is a characteristic laser frequency. The coupling of particles to laser envelopes is a common model in free electron laser (FEL) simulations. The first application of this numerical technique to Raman backscatter in a plasma was published by Shvets *et al.*[15] In this work, the longitudinal electric field was calculated using a harmonic decomposition of the electron bunching parameter, a common technique in FEL simulations. In contrast, our model uses a PIC-style algorithm to calculate the longitudinal field, and each spatial ponderomotive wavelength can be individually mod-

eled. The earlier work[15] did not study thermal effects on the pulse amplification and compression.

Other hybrid-type codes which combine the envelope and PIC models are reduced PIC,[16] quasistatic PIC,[17] and turboWAVE.[18] The reduced-PIC code is designed to study parametric decay instabilities and the scattering of lasers in plasmas. In this code, the transverse current is modeled in an identical manner as fluid simulations, namely, as the product of the plasma density envelope and laser vector potential. The feature of reduced-PIC is that the instantaneous density profile is calculated using a PIC method from which a density envelope is extracted and used for the transverse current. Our code is different from the reduced PIC in the method of laser-plasma coupling. Instead of calculating the plasma density envelope, we directly couple the laser envelope to the particle current by spatially averaging over a ponderomotive bucket. In this sense, our code can be called an averaged PIC (aPIC). The quasistatic PIC and turboWAVE[17,18] is used for studying wake field generation by a single laser pulse or an electron beam. In those simulations, the laser evolves by forward scattering off of the ponderomotively excited, long wavelength plasma wave. Because the scattered wave is within the bandwidth of the mother wave with which it copropagates, a single complex laser envelope is sufficient to capture the laser evolution. While our code bears some resemblance to this model, the main difference arises because we have two counter-propagating lasers with different frequencies. We therefore need two laser envelopes which are evolved simultaneously and self-consistently. The plasma wave, with its wavelength $\sim 0.5\lambda_{\text{laser}}$, also has much finer structure, requiring a simulation spatial grid of similar resolution.

Temperature effects on RBS have been widely studied. For example, considerable experimental, analytical, and numerical studies of RBS in a high temperature plasma, where Landau damping is significant, have been performed at Los Alamos National Laboratory.[19–21] The motivation for that research was to increase laser absorption on target by reducing the RBS reflectivity. It was anticipated that Landau damping, which generally suppresses plasma wave excitation, would also significantly suppress RBS. It was observed experimentally, however, that reflectivity in a warm plasma was not as small as theory predicted.[19] This phenomenon was analyzed and simulated by Vu *et al.*[20,21] utilizing their reduced-PIC code. They attributed the unexpectedly large Raman backscattering in a warm plasma ($T_e = 4-6$ keV) to reduced damping by trapped particles.[12]

Our study of RBS has a different motivation. We desire to enhance and control RBS, rather than to suppress it, so as to maximize laser pulse amplification. Our code is tailored for this specific purpose by including two dominant laser modes: the first is the pumping laser that delivers the energy, the second is the down-shifted seed that extracts the energy into a short, amplifying pulse. A moving window is implemented to save computational cycles, and the code is parallelized for the IBM SP at NERSC.

We observed good agreement between the aPIC and a full PIC code [XOOPIC (Ref. 22)] in the linear regime of RBS. To benchmark the code in the nonlinear regime, we compared our results with those obtained using the three-wave model rather than the full PIC, which are extremely computationally expensive for the runs of interest. In a cold plasma, no significant kinetic effects arise below the Langmuir wave breaking limit, and full PIC simulations have been shown to yield nearly the same results as those obtained from the three-wave equations.[8,14] Indeed, comparison of the PIC amplified pulse with the nonlinear π-pulse solutions[8] of the three-wave equations resulted in excellent agreement.

Our preliminary simulations of thermal effects on Raman amplification show that moderate temperatures, for which Landau damping is negligible, can lower the efficiency of Raman pulse amplification. Studies indicate this is related to phase shifts in the plasma wave induced by trapped particles. At high temperatures, on the other hand, the kinetic code indicates large pulse growth, while solutions of the three-wave equations with plasma wave damping corresponding to linear Landau levels exhibit almost no amplification. Understanding in detail the discrepancy between the fluid and kinetic models, especially in the particle trapping regime, is important. Further research on kinetic effects may lead to new corrections to the RBS fluid model and analysis.

This paper is organized as follows: In Sec. II, a detailed description of the numerical modeling is presented. Actual numerical schemes realizing the modeling follow in Sec. III. Benchmarking of the code for typical Raman amplification problems is presented in Sec. IV, where the code is compared with both a full PIC code and with numerical solutions to the three-wave equations. In Sec. V, we address thermal effects in pulse amplification and compression. Finally, we provide conclusions in Sec. VI.

II. DERIVATION OF AVERAGED EQUATIONS FOR THE APIC SIMULATION

In this section, we derive envelope equations for the lasers and their coupling to the averaged particle current. The one-dimensional wave equation for a laser vector potential $\vec{A}_L$, is in the Coulomb gauge $\vec{\nabla}\cdot\vec{A}_L = 0$

$$-\frac{\partial \vec{A}_L^2}{\partial z^2} + \frac{1}{c^2}\frac{\partial^2 \vec{A}_L}{\partial t^2} = \frac{\vec{J}_\perp}{c^2 \epsilon_0}. \tag{1}$$

In Eq. (1), the laser vector potential is driven by the transverse current. The longitudinal plasma current does not directly couple to the laser envelopes. The vector potential for each wave is expressed in terms of a normalized, slowly varying, complex-valued amplitude a, defined by $A = (mc/e)a \exp[i(\pm kz - \omega t)]$, where the $+/-$ signs are for the seed and pump lasers, respectively. Thus

$$\vec{A}_L = \frac{mc}{2e}(\vec{a}_1 e^{i\phi_1} + \vec{a}_2 e^{i\phi_2}) + \text{c.c.}, \tag{2}$$

where the subscript 1 (2) represents the seed (pump), $\phi_1 = k_1 z - \omega_1 t$ and $\phi_2 = -k_2 z - \omega_2 t$. Inserting Eq. (2) into Eq. (1) yields

$$\left[-i\omega_1\left(\frac{\partial}{\partial t}+\frac{c^2k_1}{\omega_1}\frac{\partial}{\partial z}\right)+\frac{(c^2k_1^2-\omega_1^2)}{2}\right]a_1e^{i\phi_1}$$
$$+\left[-i\omega_2\left(\frac{\partial}{\partial t}-\frac{c^2k_2}{\omega_2}\frac{\partial}{\partial z}\right)+\frac{(c^2k_2^2-\omega_2^2)}{2}\right]a_2e^{i\phi_2}+\text{c.c.}$$
$$=\frac{eJ_\perp}{mc\epsilon_0}, \tag{3}$$

where we omitted the second derivatives of the slowly varying envelopes. We have also omitted the vector notation since $J_\perp$ and $a_{1,2}$ are parallel to each other. Equation (3) can be separated into envelope equations of the seed and pump by multiplying $e^{-i\phi_{1,2}}$ and integrating over a ponderomotive wavelength of the counter-propagating lasers $[\lambda_b=2\pi/(k_1+k_2)\simeq 0.5\lambda_{1,2}]$. Averaging over fast oscillations, then, yields

$$-i\omega_1\left(\frac{\partial a_1}{\partial t}+\frac{c^2k_1}{\omega_1}\frac{\partial a_1}{\partial z}\right)+\frac{(c^2k_1^2-\omega_1^2)}{2}a_1$$
$$=\frac{e}{mc\epsilon_0\lambda_b}\int_{\lambda_b}J_\perp e^{-i\phi_1}\mathrm{d}z \tag{4}$$

and

$$-i\omega_2\left(\frac{\partial a_2}{\partial t}-\frac{c^2k_2}{\omega_2}\frac{\partial a_2}{\partial z}\right)+\frac{(c^2k_2^2-\omega_2^2)}{2}a_2$$
$$=\frac{e}{mc\epsilon_0\lambda_b}\int_{\lambda_b}J_\perp e^{-i\phi_2}\mathrm{d}z. \tag{5}$$

The average transverse current can be derived using conservation of transverse canonical momentum:

$$\gamma_j\vec{v}_{\perp j}-\frac{e}{m}\vec{A}_L(z_j,t)\simeq 0, \tag{6}$$

where $v_{\perp j}$ is the perpendicular velocity, z_j the axial position, and γ_j is the relativistic factor of particle j. This relation is exact in a one-dimensional system. The transverse current is thus

$$J_\perp=-e\sum_j\delta(z-z_j)v_{\perp j}=-ec\sum_j\frac{\delta(z-z_j)}{2\gamma_j}(a_{1j}e^{i\phi_{1j}}$$
$$+a_{2j}e^{i\phi_{2j}}+\text{c.c.}), \tag{7}$$

where $a_{1,2j}$ are the normalized envelopes of seed and pump at $z=z_j$. From Eq. (7), the averaged current is calculated as

$$\frac{e}{mc\epsilon_0\lambda_b}\int_{\lambda_b}dzJ_\perp e^{-i\phi_1}=-\frac{\omega_p^2}{2}\left(a_1\left\langle\frac{1}{\gamma_j}\right\rangle+a_2\left\langle\frac{e^{i\phi_j}}{\gamma_j}\right\rangle\right), \tag{8}$$

and similarly,

$$\frac{e}{mc\epsilon_0\lambda_b}\int_{\lambda_b}dzJ_\perp e^{-i\phi_2}=-\frac{\omega_p^2}{2}\left(a_1\left\langle\frac{e^{-i\phi_j}}{\gamma_j}\right\rangle+a_2\left\langle\frac{1}{\gamma_j}\right\rangle\right), \tag{9}$$

where ϕ_j is the ponderomotive phase of the jth particle defined as $\phi_{2j}-\phi_{1j}=-(k_2+k_1)z_j-(\omega_2-\omega_1)t$. The amplitudes $a_{1,2j}$ are outside of the average because they are slowly varying quantities. The bracket $\langle\cdots\rangle$ is defined as

$$\langle Q_j\rangle=\frac{\Sigma_jQ_j}{N_0}, \tag{10}$$

where the subscript j goes over particles in a ponderomotive bucket and N_0 is the initial (unperturbed) number of particles in the same bucket.

In deriving Eqs. (8) and (9), we averaged over fast oscillation terms. The usual single-wave dispersion terms, $-(1/2)\omega_p^2a_1\langle 1/\gamma_j\rangle$ and $-(1/2)\omega_p^2a_2\langle 1/\gamma_j\rangle$, are assumed to be canceled by $(\omega_{1,2}^2-c^2k_{1,2}^2)a_{1,2}$ in Eqs. (4) and (5). The final form of the envelope equations are

$$\frac{\partial a_1}{\partial t}+c\frac{\partial a_1}{\partial z}=-i\frac{\omega_p^2}{2\omega_1}a_2\left\langle\frac{e^{i\phi_j}}{\gamma_j}\right\rangle, \tag{11}$$

and

$$\frac{\partial a_2}{\partial t}-c\frac{\partial a_2}{\partial z}=-i\frac{\omega_p^2}{2\omega_2}a_1\left\langle\frac{e^{-i\phi_j}}{\gamma_j}\right\rangle, \tag{12}$$

where we used $\omega_{1,2}\simeq ck_{1,2}$, valid for $\omega_p\ll\omega_{1,2}$. This is generally a good approximation for the regimes of interest in Raman amplification.

The equation of motion of a particle is derived from

$$\frac{\mathrm{d}\vec{u}}{\mathrm{d}t}=-\frac{e}{m}\vec{E}_s-\frac{e}{m}\vec{E}_f-\frac{e}{m}\vec{v}\times\nabla\times\vec{A}_L, \tag{13}$$

where $\vec{u}=\gamma\vec{v}$, E_f is the fast oscillating electric field of the lasers, and E_s the slow electrostatic plasma field. Using the vector identity $\vec{v}\times\nabla\times\vec{A}_L=(\nabla\vec{A}_L)\cdot\vec{v}-\vec{v}\cdot\nabla\vec{A}_L$, Eq. (13) is simplified to

$$\frac{\mathrm{d}\vec{P}_c}{\mathrm{d}t}=-\frac{e}{mc}\vec{E}_s-(\nabla\vec{a}_L)\cdot\vec{v}_\perp, \tag{14}$$

where P_c is the canonical momentum defined as $\vec{u}/c-\vec{a}_L$, and only the transverse component of $\vec{v}$ is kept because $\vec{a}_L$ is transverse. From $\vec{v}_\perp=c\vec{a}_L/\gamma$, and averaging over fast oscillations, Eq. (14) becomes

$$\frac{\mathrm{d}\vec{p}_s}{\mathrm{d}t}=-\frac{e}{mc}\vec{E}_s-\frac{c}{2\gamma}\nabla\left(\frac{1}{2}|a_1|^2+\frac{1}{2}|a_2|^2\right.$$
$$\left.+\Re\mathrm{e}[\vec{a}_1^*\cdot\vec{a}_2e^{i\phi_{\mathrm{PM}}}]\right), \tag{15}$$

where $\vec{p}_s$ is the slowly varying part of the canonical momentum, which equals the longitudinal momentum $(\gamma v_z/c)$. The separate derivatives of the envelopes a_1 and a_2 are neglected in our code, since $\partial_z a_{1,2}\ll k_{1,2}a_{1,2}$. These terms become important when the time scale is comparable to that of Raman forward scattering and self-modulation instabilities.[18] We consider short RBS problems where those effects are not important. aPIC code can be extended straightforwardly to be able to simulate them by including derivatives of the full $|\vec{a}|^2$.

The calculation of the electrostatic field $\vec{E}_s$ is performed using standard PIC methods.[22]

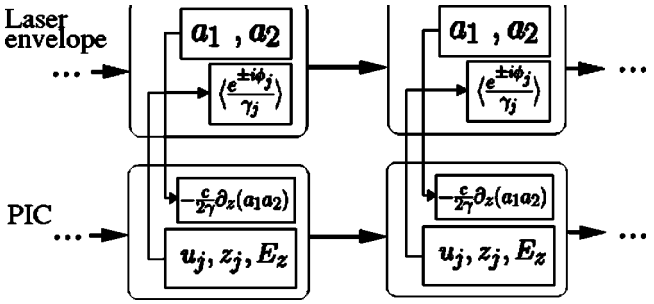

FIG. 1. Schematic of the coupling of the laser envelope solver with the particle mover and Poisson solver (PIC).

III. NUMERICAL SCHEME

In this section, we briefly describe the numerical scheme implemented in the code. The input parameters are grids, a time step, the plasma properties (density, number of simulation particles, temperature), and the laser properties (wavelength, pulse shape, values of normalized vector potentials). The simulation particles are loaded according to a bit-reversed sequence to achieve a quiet start. The main loop begins with the computation of each particle's ponderomotive phase (ϕ_j) and relativistic factor (γ_j), from which the averaged current and ponderomotive force are obtained. We then calculate the electrostatic force by the leap-frog method, and move the particles accordingly. The laser envelopes are advanced with the source term (current) obtained from the first block of the main loop. Finally, the simulation window is shifted forward to implement the moving window. The coupling between PIC part and laser envelope solver, which is the most essential part of the aPIC, is shown schematically in Fig. 1.

A. Particle loading

Using a sequence of random numbers to spatially distribute particles often results in small levels of particle bunching. This bunching generates a simulation noise level that is generally much higher than in any realistic system, since each simulation particle represents many plasma electrons. Since one of the goals is to properly model noise and thermal effects, this can become a significant problem, particularly when we wish to model pulse amplification starting from a weak seed. To alleviate this problem, we load particles in a quiet start using bit-reversed numbers to determine the initial spatial particle distribution.[22,23] We use the number 2 as a base number and typically load 128–256 particles per beat wavelength for cold plasma simulations and larger number of particles (256–512) for thermal plasmas to reduce the numerical noise.

For the initial distribution in velocity space, we used the cumulative distribution function method[22] to load a uniform Maxwellian distribution. The density of particles is therefore proportional to $\exp(v^2/v_{th}^2)$, where v_{th} is derived from $T_e = m v_{th}^2/2$.

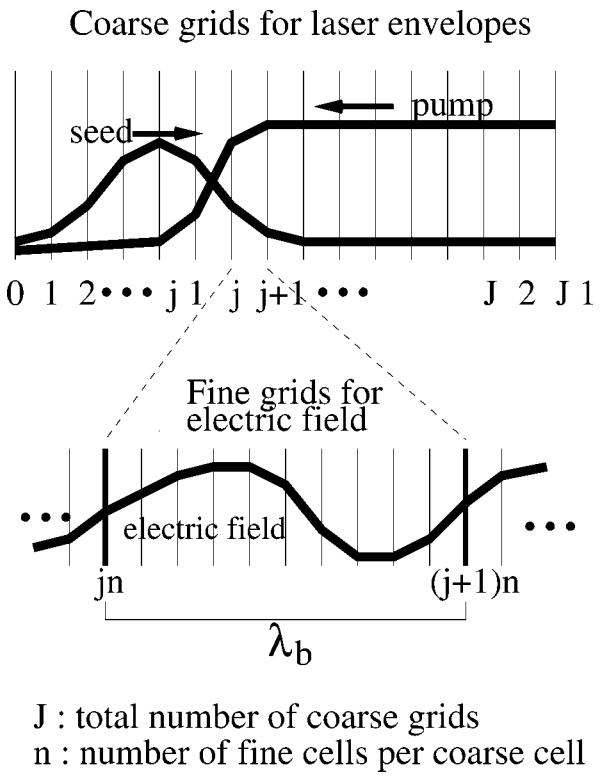

FIG. 2. Simulation grids. The longitudinal electric field is calculated on the fine grid which resolves the beat wavelength (λ_b). The coarse grid is for the calculation of laser envelopes. The size of a coarse cell equals the beat wavelength.

B. Laser and electrostatic field

The laser envelope and the electrostatic field of the plasma wave are calculated on different grid systems: coarse grids for laser envelopes and fine grids for the plasma wave (Fig. 2). The size of the coarse grid cells equal the beat wavelength; a cell size incommensurate with or smaller than the beat wavelength is not favorable, because the current, which drives the laser envelopes, should be averaged over a ponderomotive bucket. The centered-grid backward differential (BDF) method is used in the envelope solver. This method is unconditionally stable, which is appropriate for a steep problem such as Raman pulse compression. The discrete form is

$$\frac{a_i(t+\Delta t) - a_i(t)}{\Delta t} \pm c\frac{a_{i+1}(t+\Delta t) - a_{i-1}(t+\Delta t)}{\Delta z} = j_i(t), \tag{16}$$

where the subscripts are grid indices, and $\pm$ apply to the seed and pump, respectively.

The electrostatic field of the plasma wave is calculated using a fine grid, resolving the beat wavelength typically by 16 or 32 cells. The charge density at a grid point is found, for each simulation particle, by linear interpolation. The electric field is

$$\frac{E_{j+1/2}-E_{j-1/2}}{\Delta z_j}=\frac{e(N_{i,j}-N_{e,j})}{\epsilon_0}, \tag{17}$$

where N_{ij} and N_{ej} are the ion and electron density at the jth grid, respectively. We assume ions are an immobile neutralizing background, consistent with study of short pulse Raman amplification. Brillouin scattering of the laser can be included in a straightforward extension of the code by allowing for ion motion. Because Eq. (17) is a first-order differential equation, one boundary condition at the right edge of the simulation domain is sufficient to completely specify its solution. Physically, the electrostatic field at the right edge (front of the moving window) should vanish, because the plasma has not been perturbed by the seed-pump interaction, and no signal in the perturbed region can reach the moving window front (which moves with the speed of light). This simple boundary condition works well for a cold plasma, but it generates unphysical fields when simulating a thermal plasma. This is because plasmas with a nonzero temperature naturally have fluctuations in the longitudinal field due to thermal motion of the electrons. Since the moving window is not a physical boundary (such as a conductor or a dielectric) but only the simulation boundary, the electrostatic field at this boundary should have fluctuation levels consistent with the (numerically enhanced) thermal noise. If the electrostatic field at the boundary is instead set to zero, it generates noisy oscillations of a spatial direct current (dc) field in the whole domain. This dc field is purely numerical and must be avoided. To do this, we consider the last block of the coarse grids near the moving window front, which remains unperturbed by the seed laser. The electric fields at the fine grids belonging to that block are

$$E_{N-3/2}=E_{N-1/2}-Q_{N-1},$$

$$E_{N-5/2}=E_{N-3/2}-Q_{N-2}=E_{N-1/2}-Q_{N-1}-Q_{N-2},$$

$$\cdots,$$

$$E_{N-n-1/2}=E_{N-1/2}-Q_{N-1}-\cdots-Q_{N-n}, \tag{18}$$

where Q is the charge density divided by ϵ_0, N the last index of the fine grids, and n the number of fine grids per beat wavelength. Note that the electric field and the charge density Q interlace with each other. By summing,

$$\sum_{j=N-n-1/2}^{N-3/2}E_j=nE_{N-1/2}-\sum_{j=N-n}^{N-1}(n-N+j+1)Q_j. \tag{19}$$

Using the zero-dc-field condition in the unperturbed region ($\Sigma_{j=N-n-1/2}^{N-1/2}E_j=0$) in Eq. (19) yields the desired boundary condition,

$$E_{N-1/2}=\frac{\sum_{j=N-n}^{N-1}(n-N+j+1)Q_j}{n+1}. \tag{20}$$

Note that Eq. (20) reduces to $E_{N-1/2}=0$ for the cold plasma, since the thermal charge fluctuation Q_j s are zero. Numerically, Q_j s are not completely zero even in cold plasma, but the quiet start with bit-reversed scheme ensures they have a negligible value.

C. Moving window

Moving windows are a very useful technique for reducing the computational cost of short-pulse laser-plasma simulations. The technique is not a physical coordinate transformation but rather a spatial shift of the simulation domain. As the simulation window moves, data are discarded at the back of the window, shifted back by one grid within the window, and clean plasma and electromagnetic field is loaded at the window head. We found that careful thermal plasma loading at the window head is important for noise control. Loading a quiet plasma at the moving window front can result in a discontinuity in density fluctuations between the noisy plasma, that has been evolved by a couple of time steps, and the newly loaded quiet plasma. We removed the discontinuity by keeping track of a separate, supplemental, plasma block. This plasma block is one beat-wavelength long (the size of the coarse grid), and self-consistently evolves as a function of time with a periodic boundary condition and a self-consistent electrostatic field. This block is then used to load plasma at the moving window front with plasma fluctuation levels consistent with the rest of the evolved plasma.

D. Parallelization

Most of the computation effort is spent calculating particle properties, such as ponderomotive phase, current, charge allocation to the grids for the electrostatic field computation, and in the particle mover. The code runs in parallel using a scheme where we let every CPU access the whole grid system (instead of dividing the system into sections) and explicitly parallelize only the particles. This is a very effective method in one-dimensional problems, since the number of grid points is not so large (we need not worry about the memory required for the grids) and the computation time of the field solver is almost negligible. Each CPU has its own particles distributed throughout the whole system, and calculates their ponderomotive phase, relativistic γ factor, and current, which are the most computationally intensive processes. The current at each CPU is summed to find the total current. The plasma density is also calculated by the individual CPU's and summed. The electrostatic field is computed at one CPU and redistributed to others for particle moving, which is another time consuming routine. The parallelization efficiency tested was about 95%, meaning that 16 CPU's resulted in a speed up by a factor of 15.3.

IV. BENCHMARKING OF THE APIC CODE

We first compare our code with the one-dimensional particle-in-cell code XOOPIC (Ref. 24) in the linear regime and with the numerical solution of the three-wave equations[8] in the pump-depletion regime. In both regimes, we used a cold plasma only. The thermal plasma case will be discussed in the following section.

Figure 3 shows the seed amplification in the linear regime. We used a pump of higher frequency and larger amplitude than the seed amplitude to observe Raman amplification in the fixed-pump (linear) regime. For a pump whose amplitude is much larger than the seed, energy transfer is

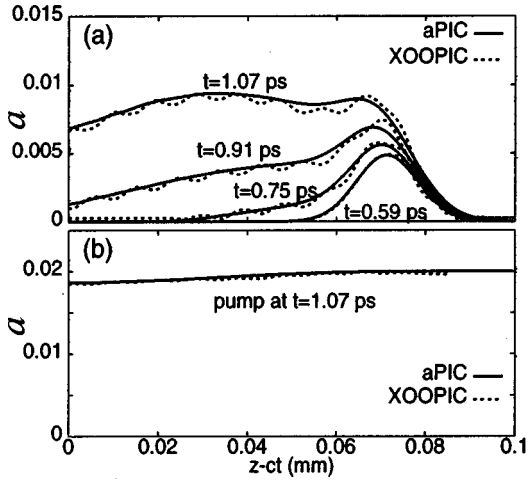

FIG. 3. Pulse amplification by the RBS in the linear regime. The simulations were performed with $a_{\text{seed}}=0.005$, $a_{\text{pump}}=0.02$, $\lambda_{\text{seed}}=1\mu$m, $\lambda_{\text{pump}}=0.9\mu$m, $\omega_p=2.094\times10^{14}$ rad/s (corresponding to a plasma density of 1.38×10^{19} cm^{-3}), and an initially Gaussian seed laser $a_{\text{seed}}\exp[-t^2/\sigma^2]$ with $\sigma=9.47\mu\text{m}=10\lambda_b$. Two simulations are compared (solid lines from the aPIC code and dashed lines from XOOPIC) at different times. (a) The seed pulse (right-going) and (b) pump (left-going) profiles are plotted. The ordinate represents the normalized vector potential ($a\equiv eA/mc$). The position of the seed and pump is relative to the moving window, i.e., $z-ct$.

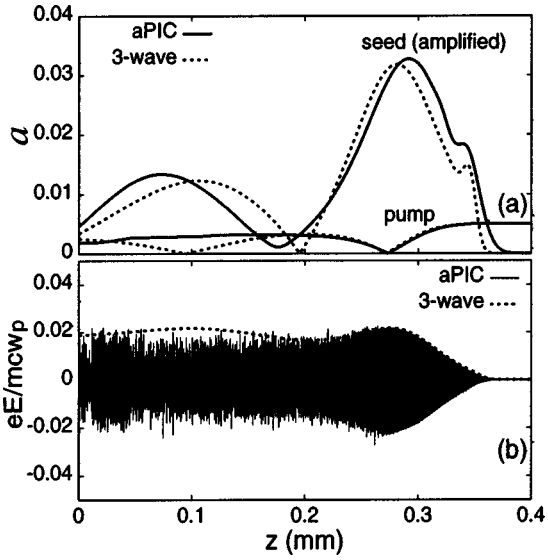

FIG. 4. Raman amplification and compression of the seed pulse in the pump depletion regime. The solid lines are from the kinetic simulation code aPIC, while the dotted lines are from numerically solving the three-wave equations. The parameters used are $a_{\text{pump}}=0.005$, initial $a_{\text{seed}}=0.01$, the plasma density $n_e=1.38\times10^{19}$ cm^{-3} corresponding to $\omega_p=2.1\times10^{14}$ rad/s$=\omega_{\text{pump}}-\omega_{\text{seed}}$ (on resonance), and an initially Gaussian seed profile $a_{\text{seed}}\exp[-t^2/\sigma^2]$ with $2\sigma=33\lambda_b\simeq52$ fs. (a) The amplified seed measured at $t=10$ ps and (b) the plasma wave at the same time. The leading peak of the seed has a good agreement between the kinetic and three-wave calculations. The numerical noise of the kinetic simulation generates some discrepancy in the tail.

almost completely in one direction: from the pump to the seed.[9] The linear growth of the seed for various conditions is well known.[8] Two simulations with the one-dimensional XOOPIC (Ref. 22) and the aPIC code are in excellent agreement with each other. The wiggling in the seed profile of XOOPIC originated from an imprecise diagnostic separation of the right- and left-going waves.[25]

The pump laser begins to be depleted as the seed pulse grows and nonlinear interaction between the three waves starts. In this regime, where the seed amplitude is significant, the back of the seed gives energy to the pump, resulting in pulse compression (i.e., π-pulse[8]). Figure 4 shows the amplification and compression of the seed laser and the depletion of the pump. We benchmarked the results from the aPIC code with the numerical solution of the corresponding three-wave equations:

$$\frac{\partial a}{\partial t}-c\frac{\partial a}{\partial z}=-Kbf,\quad \frac{\partial b}{\partial t}+c\frac{\partial b}{\partial z}=Kaf,$$
$$\frac{\partial f}{\partial t}+i\delta\omega f+\nu f=Kab, \tag{21}$$

where $K=\sqrt{\omega_p}c(k_0+k_1)/4\sqrt{\omega_0\omega_1}$, $a=\sqrt{\omega_0}a_{\text{pump}}$, $b=\sqrt{\omega_1}a_{\text{seed}}$, and $f=\sqrt{\omega_p}eE/m\omega_p v_{\text{ph}}$, with v_{ph} the phase velocity of the plasma wave. The detuning is defined as $\delta\omega=\omega_p+\omega_{\text{seed}}-\omega_{\text{pump}}$ and ν is a damping coefficient (typically calculated from Landau damping). We do not consider collisional damping. Equation (21) was solved with a fourth-order Runge-Kutta method. The profiles of the first main peaks in Fig. 4 agree well with each other. There is a small discrepancy in the profiles of the second peaks, which comes from the numerical noise of the aPIC calculations. This can be further reduced by increasing the number of particles and/or decreasing the simulation time step. The plasma wave profile from the aPIC code, Fig. 4(b), shows some noise in the tail, while its front is regular and in good agreement with the envelope from the three-wave equations.

V. REDUCED RBS COUPLING IN THERMAL PLASMA

Our aPIC code has significant advantages over PIC codes in the study of RBS in thermal plasmas. Even in the one-dimensional case, systematic simulation studies of thermal RBS with PIC codes is challenging, since many more simulation particles are required, as compared to the cold plasma case, to model the temperature effects with an acceptable level of numerical noise.

An obvious effect of temperature in RBS is the introduction of Landau damping, which suppresses the growth of the Langmuir wave, resulting in reduced energy transfer from the pump to the seed. Other studies of thermal RBS by Vu *et al.*, however, indicate that linear Landau damping is only part of the story. Using the reduced-PIC code[16] they observed an RBS reflectivity considerably larger than predictions based on a fixed damping coefficient, which they attributed to reduced damping by trapped particles.[21] Kinetic effects are also important in Langmuir wave breaking, where electrons begin to be trapped in the ponderomotive potential. Landau damping, of course, does not model kinetic effects in the particle trapping regime.

We choose parameters such that linear Landau damping is negligible, and find that the trapping of particles has an effect opposite to what one might conclude from the high temperature case: a moderate to low electron temperature

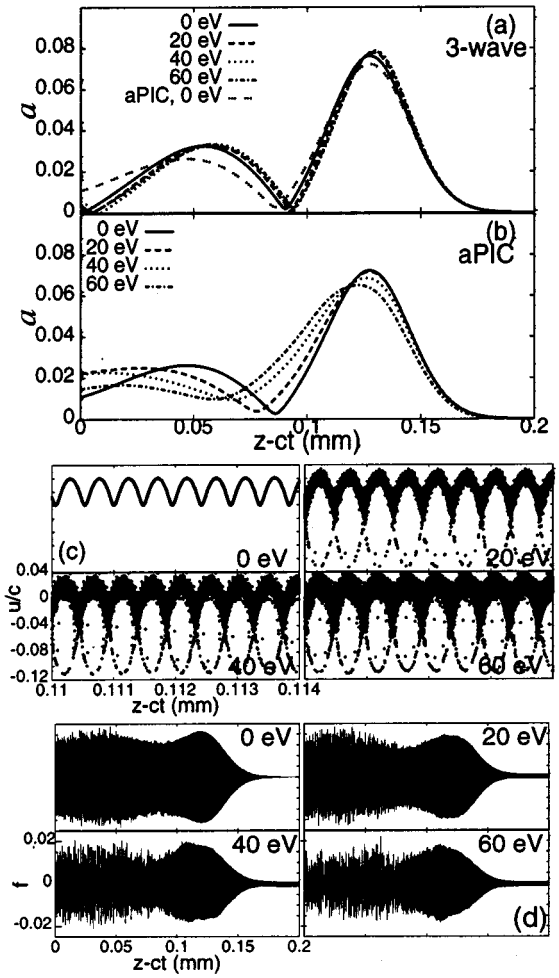

FIG. 5. Raman amplification in the thermal plasma. (a) Seed profiles from the numerical solutions of the three-wave equations, overlaid by a kinetic result for 0 eV case, and (b) the kinetic results for thermal plasmas. The measurement was done at $t=19$ ps. The laser detuning, initial shape of the seed and intensity, and the pump intensity are same as in Fig. 4. The temperature in the three-wave model is not an actual kinetic effect, but reflected as Landau damping coefficient and a detuning by the thermal correction to the plasma frequency. The three-wave solutions are almost identical because the damping is very small. The discrepancy between the three-wave and kinetic result becomes large as the temperature increases. (c) The electron phase near the leading peak of the seed, and (d) the plasma waves (in the whole simulation region), where the electric field is rescaled as $f=eE_z/mc\omega_p$.

leads to a reduction in the RBS coupling. Figure 5 shows a comparison of Raman amplification for a cold plasma and thermal plasmas with $T_e=20$, 40, and 60 eV. The parameters for the cold plasma are the same as in Fig. 4. The phase velocity of the plasma wave is $v_\phi=\omega_{th}/2k\sim 0.05c$ and the electron thermal velocity for $T_e=60$ eV is $v_{th}=\sqrt{2T_e/m}\simeq 0.015c$. The resonance for Landau damping occurs in the very tail of the Gaussian distribution. The linear Landau damping coefficient for $T_e=60$ eV is $\nu\sim 5.7\times 10^{-4}\omega_p$, much smaller than the linear RBS growth rate, $a_0\sqrt{\omega_p\omega}/2\sim 0.01\omega_p$. Landau damping is negligible for these thermal RBS simulations, and the three-wave solutions with a phenomenological damping term in Eq. (21) predicts almost no difference from the cold RBS simulations, as seen in Fig. 5(a). The small difference is mostly from the thermal correction to the plasma frequency ($\omega_{\rm th}=\sqrt{\omega_p^2+1.5v_{\rm th}^2k^2}$), rather than from the damping. The overlaid aPIC result is in very good agreement with the three-wave calculations. Figure 5(b) plots the aPIC thermal plasma results, where it is seen that as the temperature increases, there is reduced amplification and a broader leading peak of the amplified pulse. We speculate that the difference between the three-wave calculation and the kinetic results are attributed to a phase change of the plasma wave induced by particle trapping. Figure 5(c) shows the electron phase space near the leading peak, where trapping is observed in thermal plasmas. The phase shift of the plasma wave by the trapped particles can suppress efficient energy exchange between the three waves. Other sources of phase shifts, such as relativistic detuning,[26] or nonlinear thermal corrections[27,28] are not likely to be prominent in our runs. The electron velocity, which is roughly of the same order as the phase velocity of the plasma wave ($\sim 0.05c$), is nonrelativistic. The nonlinear thermal correction, which can be calculated from the formula in Ref. 28, is very small for the plasma wave amplitude $eE/mc\omega_p\sim 0.02$ for Fig. 5(d). This amplitude roughly matches the theoretical estimate[10] for thermal wavebreaking amplitude $eE/mc\omega_p=0.023-0.015$ for $T_e=20-60$ eV.

The discrepancy between the three-wave model and the aPIC simulation is significant for high-temperature plasmas, where Landau damping is strong. Figure 6 plots the case of $T_e=320$ eV, with other parameters being the same as in Fig. 5. The coefficient of linear Landau damping is now $\sim\omega_p$, while the linear growth rate of the Raman instability is $\sim 0.01\omega_p$. Because of the high damping, the three-wave calculation predicts almost no growth of the seed. The aPIC code, however, shows a mild amplification in the tail of the seed. This is consistent with other observations[21] that Landau damping is not important when the particles are trapped in the plasma wave. The trapped particles are seen in Fig. 6(b).

VI. CONCLUSION

An eikonal laser model combined with time-averaged particle motion allows fast time scales ($\leqslant 1/\omega_{\rm laser}$) to be eliminated, resulting in an efficient, fully kinetic laser-plasma simulation which has been implemented for Raman backscatter studies. Additional computational efficiency results from the use of a moving window to define the simulation domain.

We benchmarked aPIC against 1D XOOPIC in the linear regime and with the solution of three-wave equations in the pump depletion regime, obtaining good agreement. The speedup in computation from a normal PIC code, for the same plasma parameters with the same number of particles and mesh points is of order $\omega/\omega_p\sim 10$ for cases of interest. We studied the effect of plasma temperature in RBS. Reduced pulse compression was observed in a mildly thermalized plasma. A corresponding change was not observed in the three-wave calculations with same parameters. In the high temperature regime, the seed amplification is highly suppressed. However, we observed a larger Raman growth in the kinetic simulation than in the three-wave calculation with a phenomenologial damping coefficient. This result is con-

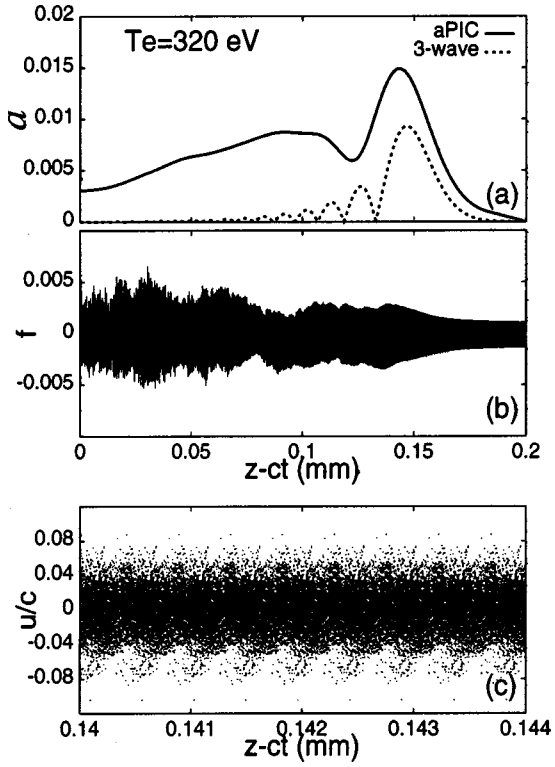

FIG. 6. Raman amplification for $T_e = 320$ eV. The laser detuning is matched to the thermally corrected plasma frequency ($\omega_{\text{th}}^2 = \omega_p^2 + 1.5\nu_{\text{th}}^2 k^2$) by lowering the pump frequency. All other parameters, except the pump frequency and the temperature, are same as in Fig. 5(a). The three-wave solution at $t = 18.7$ ps shows almost no amplification of the seed due to the severe damping. There is a moderate amplification in the kinetic simulation, because Landau damping is not effective in the particle trapping regime. This result is consistent with the observations in other contexts. (b) The plasma wave ($f = eE_z/mc\omega_p$) and (c) the phase space of electrons near the leading peak of the seed.

sistent with other experimental and simulational observations. In both the mildly and strongly thermalized RBS simulations, particle trapping plays a crucial role. The aPIC code lends itself to straightforward extension to two and three spatial dimensions. Future work includes the exploration of the influence of thermal effects on saturation of pulse amplitudes, and the development of improved fluid models that include thermal effects such as particle trapping.

ACKNOWLEDGMENTS

We acknowledge W. Fawley's helpful comments on numerical schemes.

This work is supported by DARPA and the US Department of Energy, Division of High-Energy Physics.

[1] S. E. Bodner, D. G. Colombant, J. H. Gardner *et al.*, Phys. Plasmas **5**, 1901 (1998).
[2] J. D. Lindl, Phys. Plasmas **2**, 3933 (1995).
[3] T. Tajima and J. M. Dawson, Phys. Rev. Lett. **43**, 267 (1979).
[4] E. Esarey, P. Sprangle, J. Krall, and A. Ting, IEEE Trans. Plasma Sci. **24**, 252 (1996).
[5] M. Tabak, J. Hammer, M. E. Glinsky *et al.*, Phys. Plasmas **1**, 1626 (1994).
[6] D. Strickland and G. Mourou, Opt. Commun. **56**, 219 (1985).
[7] V. M. Malkin, G. Shvets, and N. J. Fisch, Phys. Rev. Lett. **82**, 4448 (1999).
[8] V. M. Malkin, G. Shvets, and N. J. Fisch, Phys. Plasmas **7**, 2232 (2000).
[9] D. J. Kaup, A. Reiman, and A. Bers, Rev. Mod. Phys. **51**, 275 (1979).
[10] T. P. Coffey, Phys. Fluids **14**, 1402 (1971).
[11] B. I. Cohen and A. N. Kaufman, Phys. Fluids **20**, 1113 (1977).
[12] T. O'Neil, Phys. Fluids **8**, 2255 (1965).
[13] G. J. Morales and T. O'Neil, Phys. Rev. Lett. **28**, 417 (1972).
[14] D. S. Clark and N. J. Fisch, Phys. Plasmas **10**, 4848 (2003).
[15] G. Shvets, J. S. Wurtele, and B. A. Shadwick, Phys. Plasmas **4**, 1872 (1997).
[16] H. X. Vu, B. Bezzerides, and D. F. DuBois, J. Comp. Physiol. **156**, 12 (1999).
[17] C. Huang, V. Decyk, S. Wang, E. S. Dodd, C. Ren, W. B. Mori, T. Katsouleas, and T. Antonsen, Jr., *Proceedings of the 2001 Particle Accelerator Conference, Chicago, 2001*, edited by P. W. Lucas and S. Weber (IEEE), Vol. 5, p. 4005; J. H. Cooley, T. M. Antonsen, Jr., C. Huang, V. Decyk, S. Wang, E. S. Dodd, C. Ren, and W. B. Mori, in *Proceedings of Advanced Accelerator Concepts Tenth Workshop, Mandalay Beach, 2002*, edited by C. E. Clayton and P. Muggli (American Institute of Physics, New York), p. 232.
[18] D. F. Gordon, W. B. Mori, and T. M. Antonsen, Jr., IEEE Trans. Plasma Sci. **28**, 1135 (2000).
[19] J. C. Fernandez, J. A. Cobble, D. S. Montgomery, M. D. Wilke, and B. B. Afeyan, Phys. Plasmas **7**, 3743 (2000).
[20] H. X. Vu, D. F. DuBois, and B. Bezzerides, Phys. Rev. Lett. **86**, 4306 (2001).
[21] H. X. Vu, D. F. DuBois, and B. Bezzerides, Phys. Plasmas **9**, 1745 (2002).
[22] C. K. Birdsall and A. B. Langdon, *Plasma Physics via Computer Simulations* (McGraw-Hill, New York, 1985).
[23] J. M. Hammersley and D. C. Handscomb, *Monte Carlo Methods* (Methuen, London, 1964).
[24] H. Usui, J. P. Verboncoeur, and C. K. Birdsall, IEICE Trans. Electron. **E83C**, 989 (2000).
[25] P. J. Mardahl, H. J. Lee, G. Penn, J. S. Wurtele, and N. J. Fisch, Phys. Lett. A **296**, 109 (2002).
[26] M. N. Rosenbluth and C. S. Liu, Phys. Rev. Lett. **29**, 701 (1972).
[27] E. Infeld and G. Rowlands, J. Phys. A **12**, 2255 (1979).
[28] B. K. Shivamoggi, *Introduction to Nonlinear Fluid-Plasma Waves* (Kluwer Academic, Dordrecht, 1988).